Proceedings of the World Congress on Engineering 2008 Vol II
WCE 2008, July 2 - 4, 2008, London, U.K.

Heuristic Methods for Parameter Estimation in a Smart Beam Structure

Jeoffrey T. Libo-on * Jose Ernie C. Lope † Ricardo C.H. del Rosario ‡

Abstract—**We employed the genetic algorithm and its hybrid which is a combination with the steepest descent method in estimating the parameters of a smart beam structure consisting of a cantilever beam bonded with a pair of piezoceramic patches. The estimated parameters were the density, stiffness and internal damping of both the beam and piezoceramic patches and the dielectric constant of the patches. The performance of these heuristic methods were compared with the Nelder-Mead method, a direct search method.**

Keywords: parameter estimation, smart beam structure, heuristic methods, genetic algorithms, hybrid genetic algorithm

1 Introduction

Real-time feedback control of a cantilever beam with a piezoceramic actuator and sensor was experimentally implemented in [1]. To make the system size amenable for real time computations, the model size was reduced via the Proper Orthogonal Decomposition (POD). In [11], feedback control using frequency shaping was implemented on the same experimental system. The model parameters in [11] were estimated from experimental measurements using least squares formulation.

In this paper, we propose the use of the genetic algorithm and a hybrid extension for parameter estimation to be done "off-line", i.e., before the real-time implementation of feedback control. This optimization algorithm has the advantage of global convergence, as opposed to gradient-based methods which require an initial estimate close to the true solution. This feature is desirable for cases when book values of the parameters of the smart material structure are not available. The hybridized algorithm attempts to speed up convergence by shifting to the method of steepest descent as soon as the estimate given by the heuristic algorithm is deemed close enough to the true solution.

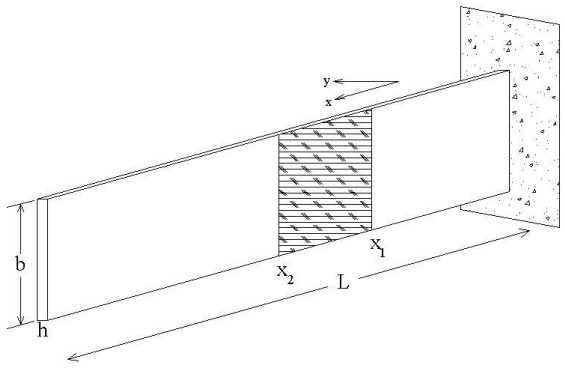

Figure 1: A Cantilever Beam

Section 2 describes the smart beam structure, presents the strong and weak forms of the equations modeling its dynamics as well as the cost functional used in parameter estimation. Section 4 outlines the numerical solution of the partial differential equation and the optimization algorithms used in parameter estimation. Sections 5 and 6 contain the numerical results and conclusions, respectively.

2 The Model

We consider a homogeneous cantilever beam bonded with piezoceramic patches (see Figure 1). In order to excite the beam, a voltage spike is induced on the patches and corresponding displacements were measured from a certain point on the beam.

2.1 Mathematical formulation

The experiment we model consists of a beam of length ℓ, width b, thickness h, density ρ, Young's modulus E and Kelvin-Voigt damping c_D. A pair of identical piezoceramic patches is attached to a portion of the beam, say at $[x_1, x_2]$, with the same length and width b. Patch parameters will be denoted by the subscript p, so that the patch thickness, width density and Young's modulus are

*Division of Physical Sciences and Mathematics, University of the Philippines in the Visayas, Miag-ao, Iloilo, Philippines Email: jtl716@yahoo.com. Research done at the University of the Philippines Diliman.

†Institute of Mathematics, University of the Philippines Diliman, C.P. Garcia Avenue, U.P. Campus, 1101 Quezon City, Philippines Tel/Fax: (63-2)-920-1009 Email: ernie@math.upd.edu.ph

‡Institute of Mathematics, University of the Philippines Diliman, C.P. Garcia Avenue, U.P. Campus, 1101 Quezon City, Philippines Tel/Fax: (63-2)-920-1009 and currently at Max Planck Institute of Biochemistry, Department of Membrane Biochemistry, Am Klopferspitz 18, 82152 Martinsried, Germany Tel: +49-89-8578-2368 Email: rcdelros@biochem.mpg.de

denoted by h_p, b_p, ρ_p, E_p and c_{D_p}, respectively.

Let $y(t,x)$ be the displacement of the beam at position x and time t. The damped Euler-Bernoulli equation is

$$\rho hb\frac{\partial^2 y}{\partial t^2} + EI\frac{\partial^4 y}{\partial t^4} + c_D I\frac{\partial^5 y}{\partial x^4 \partial t} = f(t,x),$$

where the second and third terms in the left-hand side of the equation are the stiffness and the damping terms, respectively.

However, the pair of bonded piezoceramic patches contribute to the density, damping and stiffness along the region covered by the patches. Thus the PDE describing the transverse beam vibrations with passive patch contribution is given by

$$\begin{aligned}\big(\rho hb + 2b\rho_p h_p \chi_p(x)\big)\frac{\partial^2 y}{\partial t^2} \\ + \frac{\partial^2}{\partial x^2}\Big\{\Big(EI + \frac{2b}{3}E_p a_3 \chi_p(x)\Big)\frac{\partial^2 y}{\partial x^2}\Big\} \\ + \frac{\partial^2}{\partial x^2}\Big\{\Big(c_D I + \frac{2b}{3}c_{D_p} a_3 \chi_p(x)\Big)\frac{\partial^3 y}{\partial x^2 \partial t}\Big\} \\ = \frac{\partial^2}{\partial x^2}\Big\{\frac{1}{2}E_p b d_{31}(h+h_p)(V_1(t) \\ - V_2(t))\chi_p(x)\Big\} + f(t,x). \quad (2.1)\end{aligned}$$

Here, $a_3 = (h/2 + h_p)^3 - h^3/8$ and

$$\chi_p(x) = \begin{cases}1, & x_1 \le x \le x_2 \\ 0, & \text{otherwise.}\end{cases}$$

The first and second terms on the right-hand side of Equation (2.1) are the control input and external force, respectively.

The initial conditions are

$$y(0,x) = y_0(x), \quad \frac{\partial y}{\partial t}(0,x) = y_1(x),$$

while the cantilever boundary conditions are

$$y(t,0) = \frac{\partial y}{\partial x}(t,0) = 0, \quad M_x(t,\ell) = \frac{\partial M_x}{\partial x}(t,\ell) = 0,$$

where M_x is the internal moment resultant. The latter may be simplified to

$$\begin{aligned}y(t,0) = \frac{\partial y}{\partial x}(t,0) = 0, \quad \frac{\partial^2 y}{\partial x^2}(t,\ell) = \frac{\partial^3 y}{\partial x^2 \partial t}(t,\ell) = 0, \\ \frac{\partial^3 y}{\partial x^3}(t,\ell) = \frac{\partial^4 y}{\partial x^3 \partial t}(t,\ell) = 0.\end{aligned}$$

The presence of the characteristic function χ_p in Equation (2.1) causes a discontinuity, hence a weak form of the equation will be employed in the analysis and numerical approximation.

2.2 Weak formulation and well-posedness

Let the space V of test functions be $\{\phi \in H^2(0,\ell) : \phi(0) = \phi'(0) = 0\}$. For brevity, we will write $\dot{y}(t,x)$ in place of $\partial y/\partial t$ and reserve the prime notation for derivatives with respect to x.

Multiplying both sides of (2.1) by a test function $\phi(x)$, integrating over $(0,\ell)$ and applying the boundary conditions, we obtain the following weak form of the model

Find $y(t,\cdot) \in V$ such that for all $\phi \in V$, we have

$$\begin{aligned}\int_0^\ell (\rho hb\ddot{y}(t,x))\phi(x)dx + \int_{x_1}^{x_2} 2b\rho_p h_p \ddot{y}(t,x)\phi(x)dx \\ + \int_0^\ell EIy''(t,x)\phi''(x)dx + \int_{x_1}^{x_2}\frac{2b}{3}E_p a_3 y''(t,x)\phi''(x)dx \\ + \int_0^\ell c_D I\dot{y}''(t,x)\phi''(x)dx + \int_{x_1}^{x_2}\frac{2b}{3}c_{D_p}a_3\dot{y}''(t,x)\phi''(x)dx \\ = \int_{x_1}^{x_2}\frac{1}{2}E_p b d_{31}(h+h_p)(V_1(t) - V_2(t))\phi''(x)dx \\ + \int_0^\ell f(t,x)\phi(x)dx. \quad (2.2)\end{aligned}$$

Denoting $L^2(0,\ell)$ by H, we can form the Gelfand triple $V \hookrightarrow H \cong H^\star \hookrightarrow V^\star$. To write (2.2) in an abstract form, we now define two sesquilinear forms $\sigma_1 : V \times V \to \mathbb{C}$ and $\sigma_2 : V \times V \to \mathbb{C}$ as follows

$$\begin{aligned}\sigma_1(\psi,\phi) &= \int_0^\ell EI\psi''(x)\phi''(x)dx \\ &+ \int_{x_1}^{x_2}\frac{2b}{3}E_p a_3\psi''(x)\phi''(x)dx\end{aligned}$$

and

$$\begin{aligned}\sigma_2(\psi,\phi) &= \int_0^\ell c_D I\psi''(x)\phi''(x)dx \\ &+ \int_{x_1}^{x_2}\frac{2b}{3}c_{D_p}a_3\psi''(x)\phi''(x)dx.\end{aligned}$$

Note that σ_1 and σ_2 are symmetric, continuous and V-elliptic.

For $\psi \in V$, we define $A_1\psi$ by $\langle A_1\psi,\phi\rangle_{V^\star,V} = \sigma_1(\psi,\phi)$, for all $\phi \in V$. The operator A_2 corresponding to σ_2 is defined similarly. We further define the operator $\widetilde{B} : V \to H$ by $\widetilde{B}\phi = 2(E_p b d_{31}(h+h_p))^{-1}\phi''$. We then have

$$\langle \psi, \widetilde{B}\phi\rangle_H = \langle \widetilde{B}^\star\psi,\phi\rangle_H = \langle B\psi,\phi\rangle_H,$$

where we have denoted the adjoint $\widetilde{B}^\star$ of $\widetilde{B}$ by B.

We thus obtain the following abstract formulation of (2.2) in variational form: for all $\phi \in V$, we have

$$\begin{aligned}\langle \rho hb\ddot{y}(t,\cdot),\phi\rangle_H + \langle 2b\rho_p\ddot{y}(t,\cdot)\chi_p(\cdot),\phi\rangle_H \\ + \sigma_1(y(t,\cdot),\phi) + \sigma_2(\dot{y}(t,\cdot),\phi) \\ = \langle BV_1,\phi\rangle_H - \langle BV_2,\phi\rangle_H + \langle f,\phi\rangle_H. \quad (2.3)\end{aligned}$$

Moreover, we can show that the usual inner product in $L^2(0,\ell)$ is equivalent to the following inner product in H

$$\langle \psi, \phi \rangle_p = \int_0^\ell \rho h b \psi(x)\phi(x)dx + \int_{x_1}^{x_2} 2b\rho_p h_p \psi(x)\phi(x)dx \ .$$

Now since for all $\psi \in V$ and $\phi \in H$, we have $\langle \psi, \phi \rangle_H = \langle \psi, \phi \rangle_{V^\star, V}$ and Eq. (2.3) can be written as

$$\ddot{y} + A_1 y + A_2 \dot{y} = \bar{B}u + f \in V^\star, \tag{2.4}$$

with $u = \begin{bmatrix} V_1(t) & V_2(t) \end{bmatrix}^\mathsf{T}$ and $\bar{B} = \begin{bmatrix} B & -B \end{bmatrix}$.

Finally, (2.3) can be written in the first order form as

$$\dot{z} = Az + \widehat{B}u + F \ \in V^\star, \tag{2.5}$$

where $z = \left[\begin{smallmatrix} y \\ \dot{y} \end{smallmatrix}\right]$, $A = \left[\begin{smallmatrix} 0 & I \\ -A_1 & -A_2 \end{smallmatrix}\right]$, $\widehat{B} = \left[\begin{smallmatrix} 0 \\ \bar{B} \end{smallmatrix}\right]$, and $F = \left[\begin{smallmatrix} 0 \\ f \end{smallmatrix}\right]$.

We now apply the following theorem from [2] to assert the existence, uniqueness and continuous dependence of the solution on the initial data

Theorem 2.1. *If the sesquilinear forms σ_1 and σ_2 are symmetric, continuous and V-elliptic for each $y_0 \in V$, $y_1 \in H$, then (2.4) has a unique solution $y, \dot{y} \in L^2((0,T),V)$ and $\ddot{y} \in L^2((0,T),V^\star)$. Furthermore, since the map $(y_0, y_1, \bar{B}u + F) \to (y, \dot{y})$ is continuous from $V \times H \times L^2((0,T),V^\star)$ to $L^2((0,T),V^\star) \times L^2((0,T),V^\star)$, the solution of (2.4) depends continuously on the data $(y_0, y_1, \bar{B}u + F)$.*

3 Parameter Estimation

Seven parameters of the beam were estimated, namely, the density ρ, ρ_p, the Young's modulus E, E_p, and the damping c_D, c_{D_p} of both the beam and the patches, and the dielectric constant d_{31} of the patches. The "true" values of the parameters, together with those of the measured parameters $(x_1, x_2, h, \ell, b, \hat{x})$ are given in Table 1. Since the large difference in their magnitudes could give rise to difficulties in optimization, the parameters were normalized by multiplying some constants (see Table 1).

We numerically simulated the data where the parameters used in simulation served as the true parameters of the structure. Thus, the PDE was discretized and simulated using the true parameters in Table 1, and the numerical data consisted of model displacements at the observation point $\hat{x}$. The observation or measurement at $\hat{x}$ models the proximity probe in the experimental setup of [1, 11].

Galerkin approximation was used to discretize (2.2). Cubic splines were employed as basis functions because of smoothness requirements, their accuracy and their adaptability to different boundary conditions with regard to patch contributions. For $N+1$ basis functions, the discretized PDE will give rise to a system of $2(N+1)$ first-order ordinary differential equations. The latter was solved using a stiff numerical ODE solver.

Patch parameters	**Beam parameters**
$\rho_p(\text{kg/m}^3) = 7.450 \times 10^3$	$\rho(\text{kg/m}^3) = 2.943 \times 10^{10}$
$h_p(\text{m}) = 0.00053$	$h(\text{m}) = 0.001$
$E_p(\text{N/m}^3) = 6.400 \times 10^{10}$	$E(\text{N/m}^3) = 7.062 \times 10^{10}$
$c_D(\text{Ns/m}^3) = 3.960 \times 10^5$	$c_{D_p}(\text{Ns/m}^3) = 1.04 \times 10^6$
$x_1(\text{m}) = 0.02041$	$\ell(\text{m}) = .286$
$x_2(\text{m}) = 0.04592$	$b(\text{m}) = 0.2543$
$d_{31}(\text{m/V}) = -2.62 \times 10^{-10}$	$\hat{x}(\text{m}) = 0.11076$
Normalized parameters	
$q_1 = \rho h b$	$q_2 = 2b\rho_p h_p$
$q_3 = EI$	$q_4 = \frac{2b}{3} E_p a_3$
$q_5 = c_D I$	$q_6 = \frac{2b}{3} c_{D_p} a_3$
$q_7 = \frac{1}{2} E_p b d_{31} \cdot (h + h_p)$	

Table 1: Beam and Patch parameters

In our simulations, we used $N = 16$ standard cubic splines as was done in [1]. In order to produce transverse vibrations, the voltage spikes were negatives of each other and were triangular in shape. They had a duration of 0.001 seconds with a maximum height of $100\,V$ at $t = 0.0005$ seconds. Beam displacements were measured from $t = 0$ to $t = 0.01$ at 1000 time instances.

Let us denote by y_i, $(i = 1, \ldots, 1000)$ the displacements using true parameters, and by $y_i^N(t_i, \hat{x}; q)$ the model displacements for any given set of parameters $q = [q_1, \ldots, q_7]$. We define the cost function by

$$J = \sum_{i=1}^{1000} \frac{|y_i^N(t_i, \hat{x}; q) - y_i|}{1000 \cdot \max\{|y_i|^2\}} \ . \tag{3.1}$$

The optimization problem is to find the optimal vector $q = q^*$ that minimizes the cost function J. This optimal vector q^* will now be the estimated parameters of the beam.

4 The Optimization Algorithms

The Genetic algorithm (GA) is a heuristic optimization algorithm modeled on the Darwinian principles of survival of the fittest, with a random but structured exchange of information. For a detailed treatment of this family of methods, we refer the reader to [3, 4, 7, 9]. While it is observed that GA performs well in solving optimization problems, it also requires many function evaluations and is computationally expensive. For this reason, hybrid GAs are being explored to improve performance and convergence.

In this work, we employed the standard GA and a hybrid method that combines GA with the method of steepest descent. The hybrid method was adopted from [5] and [6], incorporating some ideas about the shift from local to global searches used in [8]. The local search employed here is a first order steepest descent method with backtracking line search strategy. This method moves along the direction of the steepest gradient until some improve-

ment is found. It ends when no new point can be found (i.e., when the gradient is zero).

As in [5], we apply an adaptive way of shifting from a local search to a global search and vice versa. This can be done by introducing a coefficient of variation, the ratio of the mean evaluation of the offspring population to its corresponding standard deviation,

$$\mathrm{CV} = \frac{m}{\sigma} = \frac{\mathrm{mean}\{J(x), x \in X_0\}}{\sqrt{\mathrm{Var}\{J(x), x \in X_0\}}},$$

where J is the cost function. A local search will be called when this ratio is increasing between two successive generations (i.e., if $\mathrm{CVR} > 1$), where

$$\begin{aligned}\mathrm{CVR} &= \frac{\mathrm{CV}(i)}{\mathrm{CV}(i-1)} \\ &= \frac{\text{coefficient of variance at generation } i}{\text{coefficient of variance at generation } i-1}.\end{aligned}$$

We also applied the reduced clustering strategy. In this strategy, the population is divided into several clusters such that all associated elements of a certain cluster are closer to its centroid than to any other centroids. The local search is then applied to the best element of each cluster. During the optimization process, the number of clusters is progressively reduced so as to focus on a reduced number of local minima.

After implementing the GA and hybrid GA, we also carried out the optimization using the Nelder-Mead method, a popular non-gradient direct search method that makes use only of functional evaluations.

All algorithms were implemented using the open source numerical software Scilab.

5 Numerical Results

In Figure 2, we plot the model using parameters obtained by the GA, hybrid GA and Nelder-Mead algorithms. The displacements were taken at the observation point $\hat{x}$ and simulation time was up to 0.1 sec. A 10% noise was introduced into the data and the genetic algorithms were run using the following parameters: 30 generations, 50 individuals, mutation probability of 0.45 and cross-over probability of 0.15. Furthermore, the Nelder-Mead parameters were $\lambda_e = 2; \lambda_r = 1; \lambda_{oc} = 0.5; \lambda_{ic} = -0.5; \lambda_s = 0.5$ (see, for example, [10] for details of the Nelder-Mead algorithm).

Note that the plots of the three models in Figure 2 almost coincide with the true solution.

In Table 2, we present the true parameters and the estimated parameters from the three algorithms. As expected, the genetic algorithms took more function evaluations and longer computational time compared with

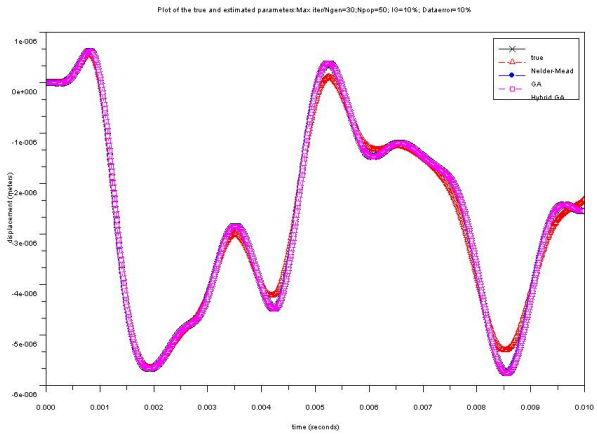

Figure 2: Plots of the model using true parameters and parameters obtained from GA, hybrid GA and the Neldel-Mead algorithms.

the Nelder-Mead algorithm, but their cost function values are lower. Furthermore, the relative error ($\|q^{true} - q^{est}\|/\|q^{true}\|$) of the estimated parameters (in the table) for Nelder-Mead, GA and hybrid GA are 0.0360932, 0.0036765 and 0.0071044, respectively.

True	**Nelder-Mead**	**GA**	**Hybrid GA**
$q_1 = 0.7484049$	0.72734373	0.74061864	0.74746874
$q_2 = 2.0082071$	2.02196142	2.03912998	1.9561229
$q_3 = 1.4965555$	1.49472319	1.48238625	1.48636416
$q_4 = 10.499967$	10.11023766	10.51907021	10.4443615
$q_5 = 0.0000220$	0.00003784	0.00002211	0.00002142
$q_6 = 0.0000650$	0.00008459	0.00006338	0.00006589
$q_7 = 0.0032620$	0.00323708	0.00324447	0.00324234
Cost (3.1)	0.00644038	0.0000104	0.00000547
CPU time (s)	228.6687	1027.3389	983.3531
Evaluations	265	1305	1476.4

Table 2: True and estimated parameters with 10% data error. Nelder-mead initial iterates are within 10% of the true parameters.

6 Conclusions

The global convergence of GA and hybrid GA make them good optimization algorithms when designing smart material structures. Even though these algorithms take more computational time, the parameter estimation can be done "off-line". Real-time parameter estimation might be necessary, e.g., due to changes in material properties in time, and for this case, the use of gradient based methods are more practical. The parameters obtained from GA or hybrid GA would be good initial guesses for the gradient based methods.

References

[1] Banks, H.T., del Rosario, R.C.H. and Tran, H.T., "Proper Orthogonal Decomposition-Based Control of Transverse Beam Vibrations: Experimental Implementation," *IEEE Transactions on Control Systems Technology*, V10, N5, pp. 717–726, 9/02

[2] Banks, H. T., Smith, R.C. and Wang, Y. *Smart Material Structures: Modeling, Estimation and Control*, Masson/Wiley, Paris/Chichester, 1996.

[3] Buckles, B., Petry, F., *Genetic Algorithm*, IEEE Computer Society Press, Los Alaminos, California, 1992.

[4] Deb, Kalyanmoy, *Multi-Objective Optimization using Evolutionary Algorithms*, Wiley & Sons, 2000.

[5] Dumas, L., Druez, B., Lecerf, N., "Adaptive Hybrid Optimization of Aircraft Engine Blades," to appear in *Journal of Computational and Applied Mathematics*.

[6] Espinoza, F.P., Minsker, B., Goldberg, D., "A Self Adaptive Hybrid Genetic Algorithm," *Proceedings of GECCO 2001*, San Francisco, California, p. 759, Morgan Kauffman Publishers, 7/01.

[7] Gen, M., Cheng, R., *Genetic Algorithms and Engineering Optimization*, John Wiley & Sons, New York, NY.

[8] Hacker, K., Eddy, J., Lewis, K., "Efficient Global Optimization Using Hybrid Genetic Algorithms," *9th AIAA/ISSMO Symposium on Multidisciplinary Analysis and Optimization*, Atlanta, Georgia, 9/02.

[9] Haupt, R. and Haupt, E., *Practical Genetic Algorithms*, John Wiley and Sons, 2004.

[10] Lagarias, J.C., Reeds, J.A, Wright, M.H. and Wright, P.E., "Convergence Properties of the Nelder-Mead Simplex Method in Low Dimensions", *SIAM J. Opt.*, V9, N1, 98.

[11] Lewis, B.M. and Tran, H.T., "Real-time implementation of a frequency shaping controller on a cantilever beam," *Applied Numerical Mathematics*, V57, pp. 778–790, 8/06